John von Neumann Institute for Computing

Structural Patterns in Ge/Sb/Te Phase-Change Materials

J. Akola, R. O. Jones

published in

NIC Symposium 2008,
G. Münster, D. Wolf, M. Kremer (Editors),
John von Neumann Institute for Computing, Jülich,
NIC Series, Vol. **39**, ISBN 978-3-9810843-5-1, pp. 169-176, 2008.

http://www.fz-juelich.de/nic-series/volume39

Structural Patterns in Ge/Sb/Te Phase-Change Materials

Jaakko Akola[1,2] **and R. O. Jones**[1]

[1] Institut für Festkörperforschung, Forschungszentrum Jülich, D-52425 Jülich
E-mail: {j.akola, r.jones}@fz-juelich.de

[2] Nanoscience Center, Department of Physics, FI-40014 University of Jyväskylä, Finland

Phase-change (PC) materials are widely used for optical recording and computer memory, but the structure of the phases involved and the nature of the phase transition in the nanoscale bits pose continuing challenges. Massively-parallel density functional simulations of the amorphous structure of the prototype materials $Ge_2Sb_2Te_5$ (GST) and GeTe show that there is long-ranged order among Te atoms in both. The crucial structural motif is a four-membered ring with alternating atoms of types A (Ge, Sb) and B (Te), an '$ABAB$ square'. The rapid amorphous-to-crystalline phase change can be viewed as a re-orientation of disordered $ABAB$ squares to form an ordered lattice, and vacancies (voids) in the disordered phases to provide the necessary space. The improved phase change performance of GST over GeTe can be correlated with the higher vacancy concentration (11.8% cf. 6.4%). Supercomputers with the power of the IBM Blue Gene/L are essential for density functional calculations of this scale and precision.

1 Introduction

Modern computers and other electronic devices place great demands on the density, speed, and stability of memory. Phase change (PC) materials already play important roles in rewritable media (CD-RW, DVD-RW, DVD-RAM, Blu-ray disc) and are prime candidates for wider applications in the future.[1] The basis of their function is the rapid and reversible transition between the crystalline and amorphous forms in nanoscale bits (~ 100 nm) of an alloy.[2] The latter arises from quenching after a localized and short (~ 1 ns) laser annealing to a temperature above the melting point T_m. Longer laser heating (~ 50 ns) to above the glass transition temperature but below T_m leads to a metastable crystal. Changes in the optical and electronic properties provide the means to monitor the transition.

The most common PC materials are Te-based alloys. The $Ge_xSb_yTe_{1-x-y}$ family provides prototypes, and $Ge_2Sb_2Te_5$ (GST) is already a commercial success in DVD-RAM (random access memory). Essential to our understanding of the properties of these materials is a knowledge of the structures of the different phases, but these are difficult to determine in binary or ternary alloys with large numbers of vacancies. Even the structure of the ordered phase of GST is controversial: Yamada[3] proposed that the metastable phase has a rock salt structure with 'Na' sites occupied randomly by Ge and Sb atoms and vacancies, and 'Cl' sites by Te. However, Kolobov et al.[4] proposed that Ge and Sb atoms are displaced from their ideal positions, enabling the order-disorder transition to occur as an 'umbrella flip' of Ge atoms from octahedral to tetrahedral positions. Most recently, x-ray fluorescence holography of an epitaxial layer of GST indicated a cubic structure with tetrahedral site symmetry about Ge atoms.[5] It is astonishing that PC materials could become the basis of commercially successful products with so much uncertainty about the structures of the phases involved.

Recent extended x-ray absorption fine structure (EXAFS) measurements on GST have found significant concentrations of Ge-Ge bonds and indications that overcoordinated Te

atoms play a role,[6] and there has been renewed focus on the role of vacancies.[7] The reverse Monte Carlo (RMC) analysis of synchrotron radiation data from amorphous (a-) GST and a-GeTe suggests that the ring structure of the former is dominated by four- and six-membered rings also seen in the crystal.[8]

DF calculations are free of adjustable parameters, but their demands on computational resources have restricted simulations on GST systems to relatively small unit cells (less than 200 atoms in all cases, less than 100 in most) and time scales that are often much shorter than those relevant experimentally. The present calculations are much larger in both number of atoms (460 for GST, 216 for GeTe) and time scale (hundreds of picoseconds). Our simulations start from liquids at 3000 K and do not favor particular crystal types. Further details of all aspects, including the electronic structure, are provided in Ref. 9.

2 Numerical Methods

2.1 Density Functional Calculations

The DF calculations were performed with the Car-Parrinello molecular dynamics package (CPMD)[10] using Troullier-Martins[11] pseudopotentials and the generalized gradient approximation of Perdew, Burke and Ernzerhof (PBE)[12] for the exchange-correlation energy functional E_{xc}. We use periodic boundary conditions, usually with one point (**k**=0) in the Brillouin zone, and the kinetic energy cutoff of the plane wave basis set is 20 Ry.

The GST simulations adopted the densities of the metastable crystalline (6.35 g/cm^3) and amorphous (5.88 g/cm^3) phases and were based on the crystalline (rock salt) structure with 512 atomic sites, where the Na and Cl sites are occupied by Ge/Sb atoms (20 % each) and vacancies (10 %), and Te atoms (50 %), respectively. The Na sites are populated randomly with Ge, Sb, and vacancies, so that the sample contains 460 atoms (102 Ge, 102 Sb, 256 Te) and 52 vacancies. The cubic cells for the c-GST and a-GST have sides of 24.05 and 24.62 Å, respectively. The GeTe system contains 216 atoms at the density of the amorphous phase (5.61 g/cm^3), and the box size is 18.61 Å. Ge, Sb, and Te are relatively heavy atoms, and we use Born-Oppenheimer MD, for which the time steps adopted (6.050 and 3.025 fs for initialization and data collection, respectively) are much longer than in the Car-Parrinello approach.

Memory of the crystalline starting structure was erased by starting the simulations at 3000 K (liquid), and details of the cooling in GST to the melting point (900 K) and to 300 K and 100 K are given in Ref. 9. Cooling and data collection in both GST and GeTe took well over 300 ps. Such relaxation times are essential for simulating structural transitions and place great demands on computing power.

2.2 Data Analysis

MD methods allow us to follow the coordinates R_i and velocities v_i of all atoms, and insight into the local order can be found from the distributions of the bond (θ_{ijk}) and dihedral angles (γ_{ijkl}). The radial distribution function (RDF) or pair correlation function $g(r)$ is a spherically averaged distribution of interatomic vectors,

$$g(r) = \frac{1}{\rho^2} \left\langle \sum_i \sum_{i \neq j} \delta(r_i)\delta(r_j - r) \right\rangle , \quad (1)$$

where ρ is the density. Partial radial distribution functions $g_{\alpha\beta}(r)$ are calculated by restricting the analysis to the elements α and β. The local structure can also be characterized by average coordination numbers found by integrating $g_{\alpha\beta}(r)$ to the first minima $R_{\min}$

$$n_{\alpha\beta} = \int_0^{R_{\min}} dr\ 4\pi r^2 \rho_{\alpha\beta}(r) g_{\alpha\beta}(r). \tag{2}$$

We calculate the structure factor $S(Q)$ by Fourier transforming the $g_{\alpha\beta}(r)$ to give the partial structure factors $S_{\alpha\beta}(Q)$, which are weighted according to the atomic fractions c_α and form factors $f_\alpha(Q)$ (for x-rays x) or the Q-independent coherent scattering lengths b_α (for neutrons n). In discussing the topology of nearest neighbours, it is convenient to separate the atoms into types A (Ge, Sb) and B (Te). It is also essential to give precise definitions of the regions where there are few atoms (vacancies, voids, cavities). Full details and the angular distribution functions are provided in Ref. 9.

Dynamical information includes the velocity autocorrelation function C_v:

$$C_v(t) = \frac{1}{N} \sum_{i=1}^{N} \frac{\langle v_i(0) \cdot v_i(t) \rangle}{\langle v_i(0) \cdot v_i(0) \rangle}, \tag{3}$$

where N is the number of particles. The self-diffusion constant for all atoms or those of species α can be determined from C_v or from the coordinates $R_\alpha(t)$.[9]

3 Results

3.1 Radial Distribution Functions and Structure Factors

The partial radial distribution functions (RDF) are shown in Fig. 1. The Te-Te curves [Fig. 1(a)] show that a-GeTe and a-GST have long-range correlations of Te atoms up to 10 Å. There are few Te-Te bonds (0.1 and 0.3 per Te atom for a-GeTe and a-GST) and the second maximum at 4.16 Å dominates. The region below 7 Å shows parallels to the ordered structure (rock salt). There are differences at larger distances, and the cubic Te sublattice proposed in the 'umbrella flip' model[4] is absent. The homopolar RDF for the remaining atoms (Ge, Sb: type A) exhibit little structure beyond ~ 6 Å.

GeTe and GST form mainly Ge-Te (and Sb-Te) bonds with pronounced first maxima in the partial RDF [Fig. 1(b)]. The Ge-Te and Sb-Te bonds are shorter than in the crystal. The location of the first minimum usually marks the limit of bond lengths, but the minima in a-GeTe and a-GST move to $3.6 - 3.9$ Å, so that there are many Ge-Te (and Sb-Te) pairs with 'intermediate' separations. The average coordination number of Te is near 3 in both a-GeTe and a-GST.

Amorphous GST has Ge-Ge, Sb-Sb, and Ge-Sb bonds with coordination numbers (Eq. 2) 0.4, 0.6, and 0.2, respectively. The EXAFS value for Ge-Ge bonds is 0.6 ± 0.2.[6] Such bonds are more common in a-GeTe, where our coordination number (1.1) compares well with an EXAFS measurement (1.2).[13] All total coordination numbers are larger than given by the '$8 - N$ rule' (Ge: 4, Sb: 3, Te: 2), and the coordination of Te atoms is lower in a-GST. The total coordination numbers are 3.4 in a-GST and 3.7 in a-GeTe.

The structure factors $S(Q)$ of a-GST have been calculated at 300 K (Fig. 2) and 900 K. There are minor differences between the $S(Q)$ calculated for neutrons and x-rays, and the

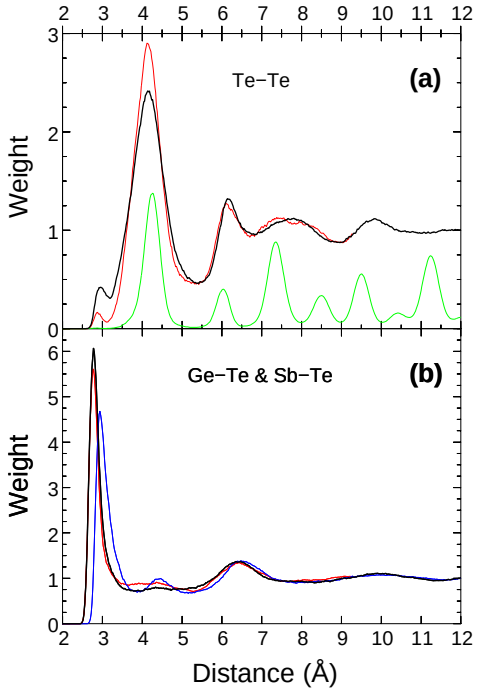

Figure 1. Radial distribution functions of a-GST and a-GeTe at 300K. (a) Te-Te. Black: a-GST, red: a-GeTe, green (scaled by 0.25): metastable GST crystal at 300 K. (b) Partial RDF. Black: Ge-Te bonds in a-GST, red: Ge-Te bonds in a-GeTe, blue: Sb-Te bonds in a-GST.

curves calculated from the total $g(r)$ (where the elements have equal weight) are also very similar. The calculated peak positions are at slightly lower Q-values than those measured, but all features are resolved. The structure factor for the amorphous phase has more structure and sharper peaks than in the liquid phase (see Ref. 9). There are more homopolar bonds (less AB alternation) and more disorder in the latter.

3.2 Ring Structures

Irreducible rings (the shortest closed loops) can be used to characterize the crystalline-amorphous phase transition, and the distributions in a-GST and a-GeTe (Fig. 3) differ: a-GST has a pronounced maximum for $n = 4$, the weight of larger rings decreases, and there is a pronounced odd-even alternation. 86% of the four-membered rings have $ABAB$ alternation, in both a-GST and a-GeTe. The bond angle distributions are peaked around 90°, and we denote these units as '$ABAB$ squares'. $60 - 80$% of Ge atoms participate in at least one such square depending on the bond cutoff distance chosen (3.2–3.4 Å).

The large number of alternating four-membered rings is evident in Fig. 4(a), where we highlight the relevant atoms and bonds in a-GST. We note the presence of $ABAB$ squares (and cubes) [Fig. 4(b)] and the relationship to the ordered $ABAB$ squares of the rock salt phase. Close to the cube in the centre of the cell there are intermediate distances where a slight re-orientation would increase the number of AB bonds and $ABAB$ squares.

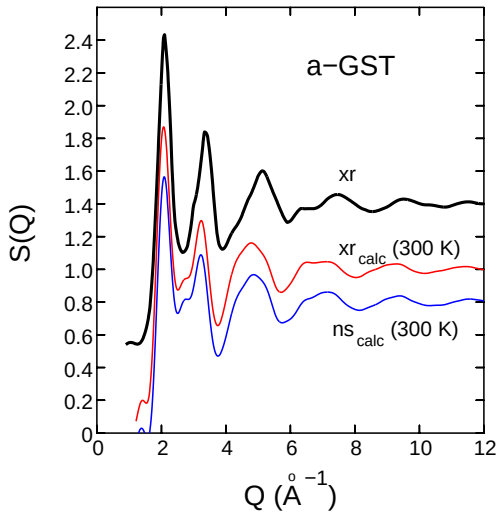

Figure 2. Structure factor $S(Q)$ of a-GST. The curve of Kohara et al. (xr, Ref. 8) is displaced by 0.4.

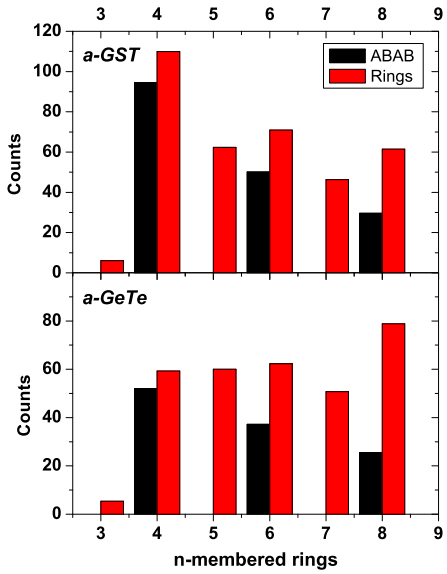

Figure 3. Statistics of irreducible n-fold ring configurations of a-GST and a-GeTe at 300 K. Black: corresponding alternating AB configurations (A: Ge/Sb, B: Te).

3.3 Vacancies

Vacancies play important roles in PC materials. The cavity analysis reveals a wide range of volumes and shapes, with a total volume of 11.8% and 6.4% for a-GST and a-GeTe,

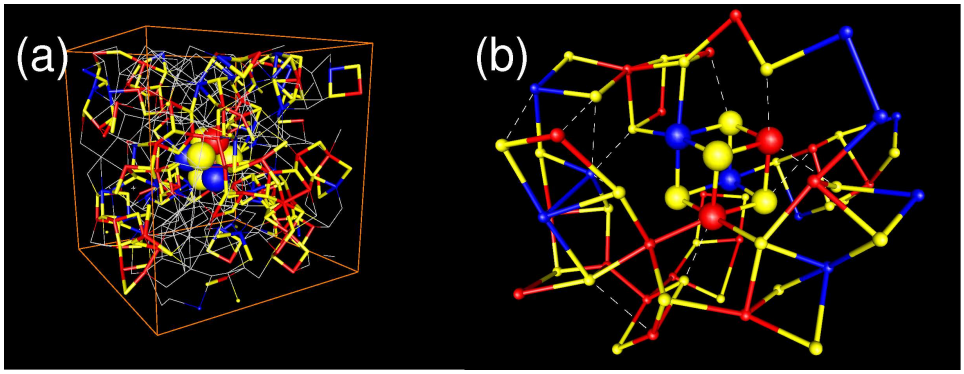

Figure 4. $ABAB$ squares and cubes in a-GST. (a) Simulation box of a-GST (24.6 Å, 460 atoms) with atoms and bonds of $ABAB$ squares and cube highlighted. Red: Ge, blue: Sb, yellow: Te. (b) Local environment of $ABAB$ cube. Dashed lines mark intermediate distances ($3.2 - 4.0$ Å).

respectively. There are then numerous vacancies in a-GeTe, whereas the ideal crystal has none. The vacancies are surrounded mainly by Te atoms, as in the crystalline phases of pseudobinary GeSbTe compounds, and a medium-sized cavity in a-GST is shown in Fig. 5(a). Sharp corners and edges are common.

The volume distribution of cavities in a-GST and the vacancy-vacancy correlation function (inset) are plotted in Fig. 5(b). There is a bias towards small cavities, and in larger vacancies (50-100 Å^3) di- and multivacancies are important and protrusions are common. There are long-range vacancy-vacancy correlations to at least 10 Å (Fig. 5(b), inset) that are similar to the behaviour in Te. Comparison of amorphous (300 K) and liquid GST (900 K) shows that the latter contains more small cavities (total volume 13.8%), but the distributions of large cavities are almost identical. Correlations are evident at 900 K (to $\sim$ 7 Å), and the dominant peak is shifted from 5.1 (300 K) to 5.7 Å (900 K). The rapid amorphous-to-crystalline transition can be viewed as a vacancy-supported reorientation of $ABAB$ squares. Numerous AB bonds are formed, but few homopolar bonds need to be broken in order to achieve crystalline order.

3.4 Diffusion

The mean square displacements of different elements at 900 K and the corresponding linear fits have been calculated. The diffusion coefficients D_α are 3.93×10^{-5} (Ge), 4.67×10^{-5} (Sb), and 3.78×10^{-5} cm^{2}s^{-1} (Te). The coordination number of Sb in the melt (3.4) is lower than in a-GST, and it is the most mobile element. The diffusion coefficients of GeTe at 1000 K are 4.65×10^{-5} (Ge) and 3.93×10^{-5} cm^{2}s^{-1} (Te), and the viscosity ranges between $1.1 - 1.2$ cP for both alloys, depending on the particle radius chosen in the Stokes-Einstein relation. The measured viscosity of liquid GeTe ranges from ~ 1.9 cP at 1000 K to 1.3 cP at 1150 K.[14]

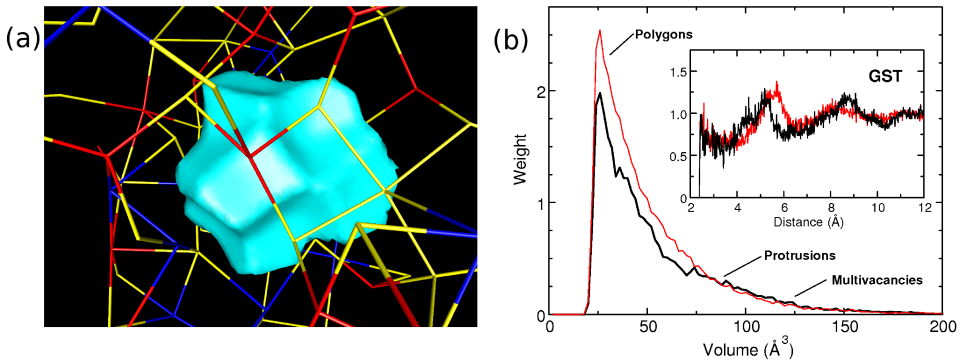

Figure 5. (a) A medium-sized cavity. (b) Volume distribution of cavities in a-GST, and (inset) vacancy-vacancy correlation function. Red: liquid at 900 K, black: a-GST at 300 K.

4 Discussion

Density functional calculations combined with molecular dynamics have been performed for liquid and amorphous GeTe and $Ge_2Sb_2Te_5$. The simulations involve 216 and 460 atoms, respectively, in the unit cell, over hundreds of picoseconds, i.e. a time scale similar to the quenching process from the liquid. Such calculations are impossible without computers with the power of the IBM Blue Gene/L. Amorphous GeTe and GST show long-range ordering of Te atoms and a high degree of alternating four-membered rings ('$ABAB$ squares') that are the main building blocks of both. Since the crystalline (rock salt) phase comprises perfectly ordered $ABAB$ squares, the rapid amorphous-to-crystalline transition can be seen as a re-orientation of $ABAB$ squares to form additional AB bonds and cubic subunits in a locally 'distorted octahedral' structure. Vacancies play a crucial role in providing the necessary space.

There are several reasons for the improved PC properties of GST relative to GeTe:

(1) *Vacancies.* The rhombohedral and fcc forms of GeTe are vacancy-free, and a-GeTe contains 6.4% vacancies by volume, about half of the value for a-GST. The local similarity between the amorphous and ordered phases is greater in GST than in GeTe due to the higher concentration of vacancies.

(2) *Homopolar bonds and AB ordering.* There are more Ge-Ge bonds in a-GeTe (1.1) than A-A bonds in a-GST (0.6 for Ge, 0.8 for Sb). This leads to different AB ordering and ring statistics, and $ABAB$ squares are more evident in a-GST.

(3) *Interatomic distances.* The first minima of the radial Ge-Te and Sb-Te distribution functions of a-GST extend to 3.8 to 3.9 Å, and these 'intermediate' distances make possible new AB bonds. This feature is less pronounced in a-GeTe, where there are fewer vacancies and the minimum is at 3.6 Å.

(4) *Atomic mobility.* The molten phases of a-GST (at 900 K) and a-GeTe (at 1000 K) have different atomic mobilities. This is due to the Sb atoms, whose diffusion constants are $\sim 20\%$ larger than those of Ge and Te.

The development of PC memory devices has favored chalcogenide semiconductors from the beginning, but current research and development focuses almost entirely on Te-

based alloys. We are now carrying out density functional simulations on both Te and the eutectic alloy $Ge_{15}Te_{85}$ in the amorphous and liquid states. The simulation cells contain up to 700 atoms, and the calculations require the power of the Blue Gene/L or its successor, Blue Gene/P.

Acknowledgments

J.A. acknowledges financial support from European Union project ULTRA-1D (NMP4-CT-2003-505457). The calculations were performed on IBM Blue Gene/L and p690 computers in the Forschungszentrum Jülich and made possible by grants from the FZ Jülich and the John von Neumann Institute for Computing (NIC).

References

1. See, for example, A. L. Greer and N. Mathur, Nature (London) **437**, 1246, 2005.
2. S. R. Ovshinsky, Phys. Rev. Lett. **21**, 1450, 1968.
3. N. Yamada, Mat. Res. Soc. Bull. **21**, 48, 1996.
4. A. Kolobov, P. Fons, A. I. Frenkel, A. I. Ankudinov, J. Tomonaga, and T. Uruga, Nat. Mater. **3**, 703, 2004, and references therein.
5. S. Hosokawa, T. Ozaki, K. Hayashi, N. Happo, M. Fujiwara, K. Horii, P. Fons, A. V. Kolobov, and J. Tominaga, Appl. Phys. Lett. **90**, 131913, 2007.
6. D. A. Baker, M. A. Paesler, G. Lucovsky, S. C. Agarwal, and P. C. Taylor, Phys. Rev. Lett. **96**, 255501, 2006.
7. See, for example, T. Matsunaga, R. Kojima, N. Yamada, K. Kifune, Y. Kubota, Y. Tabata, and M. Takata, Inorg. Chem. **45**, 2235, 2006.
8. S. Kohara, K. Kato, S. Kimura, H. Tanaka, T. Usuki, K. Suzuya, H. Tanaka, Y. Moritomo, T. Matsunaga, N. Yamada, Y. Tanaka, H. Suematsu, and M. Takata, Appl. Phys. Lett. **89**, 201910, 2006.
9. J. Akola and R. O. Jones, Phys. Rev. B **76**, 235201, 2007.
10. CPMD V3.11 Copyright IBM Corp 1990-2006, Copyright MPI für Festkörperforschung Stuttgart 1997-2001, (`http://www.cpmd.org`).
11. N. Troullier and J. L. Martins, Phys. Rev. B **43**, 1993, 1991.
12. J. P. Perdew, K. Burke, and M. Ernzerhof, Phys. Rev. Lett. **77**, 3865, 1996.
13. Y. Maeda and M. Wakagi, Jpn. J. Appl. Phys. **30**, 101, 1991.
14. V. M. Glazov, S. N. Chizhevskaya, and N. N. Glagoleva, *Liquid Semiconductors* (Plenum, New York, 1969), p. 205.